JOURNAL OF CATALYSIS **128,** 415–435 (1991)

Non-Faradaic Electrochemical Modification of Catalytic Activity

4. The Use of β''-Al_2O_3 as the Solid Electrolyte

C. G. VAYENAS,[1] S. BEBELIS, AND M. DESPOTOPOULOU

Institute of Chemical Engineering and High Temperature Chemical Processes, Department of Chemical Engineering, University of Patras, Patras GR 26110, Greece

Received March 30, 1990; revised November 15, 1990

It was found that the catalytic activity of polycrystalline Pt films deposited on β''-Al_2O_3, a Na^+-conducting solid electrolyte, can be altered dramatically and reversibly by polarizing the catalyst–solid electrolyte interface. The observed decrease in the rate of ethylene oxidation on Pt is typically $10^3 - 5 \times 10^4$ times larger than the rate of supply of Na^+ to the catalyst–electrolyte interface. A Na coverage of 0.015 suffices to cause a 70% decrease in catalytic rate which varies exponentially with catalyst work function. The latter was measured both potentiometrically and by means of a Kelvin probe. The behavior is qualitatively similar to that observed when using O^{2-}-conducting solid electrolytes and shows that the newly found effect of non-faradaic electrochemical modification of catalytic activity (NEMCA) is not restricted to any particular metal or solid electrolyte. This supports the proposed explanation of the effect which is based on the change in catalyst work function and concomitant change in chemisorptive bond strengths as a result of ion spillover upon polarization of the catalyst–solid electrolyte interface.

INTRODUCTION

It has been found recently that the catalytic activity and selectivity of metal catalyst films can be altered dramatically and reversibly by supplying or removing oxygen anions O^{2-} to or from the catalyst surface via polarized catalyst–solid electrolyte interfaces (*1–10*). The term non-faradaic electrochemical modification of catalytic activity (NEMCA) has been used to describe this new phenomenon, since the steady-state catalytic rate increase can be up to a factor of 3×10^5 higher than the steady-state rate of O^{2-} supply to the catalyst (*3, 5, 7–9*). The term "electrochemical promotion in catalysis" has also been proposed to describe NEMCA (*11*).

Previous studies of the NEMCA effect employed solid electrolyte cells of the type

gaseous reactants, metal catalyst

$$|ZrO_2(8\ \text{mol\%}\ Y_2O_3)|\ M,\ O_2, \quad (1)$$

where the metal M catalyzes the reaction

$$O_2(g) + 4e^- \rightleftharpoons 2O^{2-} \quad (2)$$

and serves as a means of supplying or removing O^{2-} to or from the porous catalyst film through the gas-impervious stabilized zirconia solid electrolyte.

The main common findings of all previous NEMCA studies (*1–10*) are the following:

I. Over wide ranges of conditions catalytic rates depend exponentially on the ohmic-drop-free (IR-free) catalyst potential V_{WR} with respect to a reference electrode

$$\ln(r/r_o) = \alpha F(V_{WR} - V^*_{WR})/RT, \quad (3)$$

where r_o is the regular, i.e., open-circuit, catalytic rate and α and V^*_{WR} are catalyst- and reaction-specific constants. The parameter α typically takes values between -1 and 1. As shown recently, both theoretically

[1] To whom correspondence should be addressed.

0021-9517/91 $3.00

(*3–5*) and experimentally (*8*) a polarization ΔV_{WR} at the catalyst–electrolyte interface causes a change $e\Delta\Phi = e\Delta V_{WR}$ to the work function $e\Phi$ of the gas-exposed catalyst surface. Consequently Eq. (3) can also be written as

$$\ln(r/r_o) = \alpha e(\Phi - \Phi^*)/k_bT, \qquad (4)$$

where Φ^* is, again, a catalyst- and reaction-specific constant.

II. The order of magnitude (typically $10–10^5$) of the enhancement factor Λ defined from

$$\Lambda = \Delta r/(I/2F), \qquad (5)$$

where Δr is the change in catalytic reaction rate and $(I/2F)$ is the rate of O^{2-} transport to or from the catalyst, can be estimated from

$$\Lambda \approx 2Fr_o/I_0, \qquad (6)$$

where I_0 is the exchange current (*3–5*) of the catalyst–solid electrolyte interface. Therefore, in order to observe strong non-Faradaic rate enhancement ($|\Lambda| \gg 1$), highly polarizable, i.e., low I_0, catalyst–solid electrolyte interfaces are required.

III. The catalytic rate relaxation time constants during galvanostatic transients are typically of the order of $2FN/I$, where N, expressed in g-atom, denotes the total catalytic surface area.

The above observations have been interpreted semiquantitatively on the basis of a uniform change of the catalyst work function induced by an electrochemically controlled spillover of ions onto the catalyst surface and of the concomitant controlled change in the strength of chemisorptive bonds (*1–11*).

In the present investigation β''-Al_2O_3, which is a Na^+ conductor (*13*), is used as the solid electrolyte, instead of Y_2O_3-doped ZrO_2, which is an O^{2-} conductor. Thus the solid electrolyte cell is of the type

gaseous reactants,

$$Pt\ |Na(I)\beta''\text{-}Al_2O_3|\ Pt,\ O_2. \qquad (7)$$

The chemistry and ion transport properties of Na(I)β''-Al_2O_3 have been reviewed thoroughly (*13*). Because of the very small currents (few μA) and reversed cell operation employed in the present study, Na^+ depletion from the solid electrolyte was not a problem even after several months of operation and thus it was not necessary to maintain the counter and reference electrodes in contact with molten Na.

The purpose of this study was to examine whether β''-Al_2O_3 can also induce the NEMCA effect and thus to examine the validity of the proposed explanation of the NEMCA effect (*1–10*). The oxidation of ethylene on Pt was chosen as a model reaction since its mechanism (*14, 15*) and NEMCA behavior using O^{2-} conducting solid electrolytes (*3, 5, 8*) have been studied in detail.

There is a rich UHV literature on the effects of alkali dopants on the chemisorptive properties of metal surfaces (*16–20*). Both UHV and atmospheric pressure studies have been reviewed thoroughly in three recent review papers (*17–19*).

EXPERIMENTAL

The experimental apparatus utilizing online gas chromatography, mass spectrometry, and IR spectroscopy for reactant and product analysis is shown schematically on Fig. 1 and has been described in detail in recent studies of NEMCA with O^{2-} conducting solid electrolytes (*1–10*). The main difference is in the nature of the solid electrolyte. A closed-at-one-end Na(I)β''-Al_2O_3 tube was used. The tube length was 10 cm and its i.d. and o.d. 1.59 and 1.90 cm, respectively. The useful reactor volume was 19.8 cm^3. The reactor cap and sealing system is identical with the one used with zirconia electrolytes (*1–10*). When not in operation, both sides of the tube were maintained in a dry synthetic air stream in order to avoid any extensive substitution of Na^+ with protons, resulting from H_2O, in the β''-Al_2O_3 lattice. With this precaution and with potentiostatic operation, as described below,

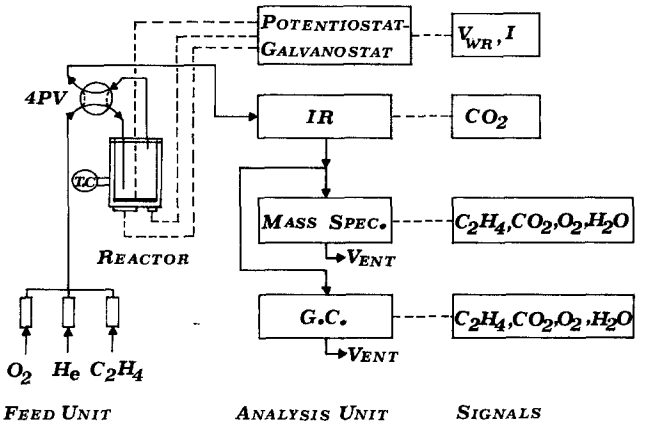

FIG. 1. Schematic diagram of the apparatus.

a tube can maintain reversible behavior over several month periods.

The porous Pt catalyst film had a superficial surface area of 2 cm^2 and was deposited on the inside bottom wall of the β''-Al_2O_3 tube as described previously (*2, 3, 5*), i.e., using a thin coating of Engelhard A1121 Pt paste followed by drying and calcining in air, first at 400°C for 2 h and then at 820°C for 20 min. Porous Pt catalyst films deposited in this mode have thicknesses of the order of 5 μm, true surface areas of the order of 500 cm^2, and have been shown by *ex situ* XPS to contain no detectable metal impurities (*2, 14, 21*). Typical scanning electron micrographs of such porous Pt catalyst films and of sections perpendicular to the Pt film-stabilized zirconia interface have been presented previously (*3*). The reactive oxygen uptake of the inside Pt catalyst film used in this investigation was 1.1×10^{-6} g-atom O, as determined by an isothermal O_2, C_2H_4 surface titration technique described previously (*14, 22*) and briefly outlined below.

Two similar porous Pt films with superficial surface areas of 1.5 and 0.1 cm^2 were deposited on the outside bottom wall of the β''-Al_2O_3 tube which was constantly exposed to dry synthetic air (Fig. 2). They functioned as counter and reference electrodes respectively. An AMEL 553 galvanostat–potentiostat was used to apply either constant currents between the catalyst and the counter electrode or constant potentials between the catalyst and the reference electrode.

Under open-circuit conditions the film exposed to the reactants acts as a regular catalyst for C_2H_4 oxidation to CO_2 and H_2O. As analyzed in Results and Discussion one of the main findings of the present work is that, as in the case of O^{2-} conducting solid electrolyte cells (*8*), the open-circuit emf V°_{WR} (measured between the catalyst and reference electrodes) *provides a direct measure of the difference in the average work func-*

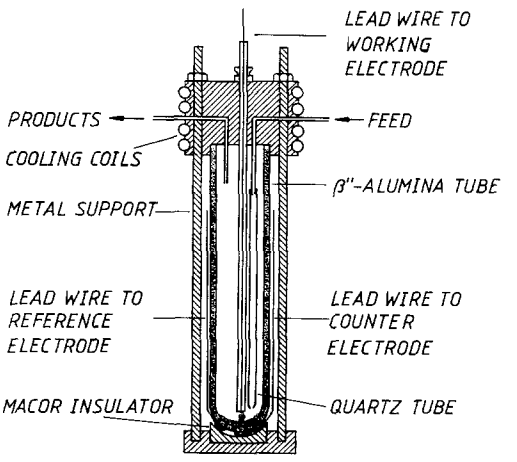

FIG. 2. Reactor configuration.

tions of the gas-exposed surfaces of the catalyst and reference electrodes. Thus, monitoring the emf enables one to monitor *in situ* the work function of the catalyst surface during reaction.

When the circuit is closed and a current I is applied between the catalyst and the counter electrode, then sodium ions Na^+ are transfered to or from the catalyst at a rate I/F. In order to maintain a notation consistent with the zirconia-based NEMCA studies (*1–10*) we denote $I < 0$ when the catalyst is negative with respect to the counter electrode, i.e., when Na^+ are supplied to the catalyst, and $I > 0$ otherwise. When current passes through the cell, the catalyst potential relative to the reference electrode V'_{WR} deviates from V°_{WR}. The difference $V'_{WR} - V^\circ_{WR}$ equals, ideally, the catalyst overpotential η (*3–5*). In practice the reference electrode is never ideal and V'_{WR} always contains a nonzero ohmic component. This component, which was typically of the order of 5–20 mV in this system, was determined via the current interruption technique in conjunction with a Hameg 205 memory oscilloscope and was subtracted from V'_{WR} in order to obtain the ohmic-drop-free (IR-free) catalyst potential V_{WR} and the catalyst overpotential η from $\eta = V_{WR} - V^\circ_{WR}$. The theoretical procedure for using η vs I data to extract the exchange current I_0 and the anodic and cathodic transfer coefficients α_a and α_c has been described in detail previously (*3, 4*).

Measurement of catalyst surface area. The following isothermal surface titration technique, also employed previously (*2–5, 21, 22*) was used to measure the reactive oxygen uptake N_O (g-atom O) of the porous Pt film: Throughout the entire procedure the catalyst is maintained at a fixed temperature T. First the catalyst is exposed to O_2 for a period t_{O_2}. Then the reactor is flushed with ultrapure He for a period t_{He} at least 8 times longer than the residence time of the reactor which is typically 3–5 s. Subsequently the catalyst is exposed to C_2H_4 (or CO) and the product CO_2 area, which provides a direct measure of chemisorbed oxygen $N_O(t_{He})$, is recorded using a mass spectrometer or IR-CO_2 Analyser. By varying t_{He} one can study the oxygen desorption kinetics. By extrapolating to $t_{He} = 0$ one can directly obtain N_O.

Work function measurement. The experimental apparatus used to measure *in situ* the work function of the gas exposed catalyst film by means of the vibrating condenser method (Kelvin probe) is shown in Fig. 3. In this design the original counter electrode, deposited on the convex side of the bottom of the β''-Al_2O_3 tube is exposed to the reactants and serves as a catalyst whereas the electrode deposited on the concave side is

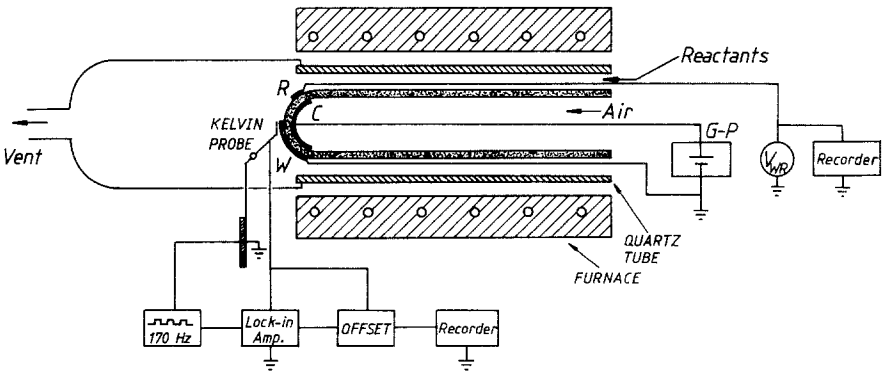

FIG. 3. Schematic diagram of the setup used to measure *in situ* the catalyst work function; G–P: Galvanostat–potentiostat; W: catalyst (working electrode); C: counter electrode; R: reference electrode.

exposed to dry synthetic air and serves as a counter electrode for closed-circuit measurements and as a reference electrode for open-circuit measurements. The catalyst work function was measured using the Kelvin method (Besocke/Delta-Phi-Electronik, Kelvin probe "S") with a 2.5-mm-diameter Au-grid vibrating condenser element ("electrode") placed ca 500 μm from the catalyst surface. It was verified that the work function (WF) measurements were not influenced by the exact distance of the two condenser elements. As shown schematically on Fig. 3 in the Kelvin probe "S" operation the contact potential difference signal is drawn from the vibrating Au grid, while the specimen (catalyst) is grounded so that the Kelvin probe Lock-in Amplifier circuit is entirely independent from the solid electrolyte cell circuit. This means that potentials applied to the cell are, of course, not fed to the Lock-in Amplifier input.

RESULTS

Open-Circuit emf and Work Function Measurements

It was recently proposed theoretically that the ohmic-drop-free potential difference in solid electrolyte cells is directly related to the work function difference of the gas-exposed surfaces of the cell electrodes (*3–5*). It was predicted that for open-circuit ($I = 0$) measurements it is

$$eV_{WR} = e\Phi_W - e\Phi_R, \qquad (8)$$

where $e\Phi_W$ and $e\Phi_R$ are the average work functions of the gas-exposed surfaces of the catalyst (W) and reference (R) electrodes, whereas for closed circuit ($I \neq 0$) measurements it is

$$\Delta eV_{WR} = e\Phi_{W(I)} - e\Phi_{W(I=0)} \qquad (9)$$

Equations (8) and (9) are valid provided the two electrodes are made of the same material and are at the same temperature (*3–5*). The validity of Eqs. (8) and (9) for O^{2-} conducting solid electrolyte cells was confirmed recently using a Kelvin probe (*8*). The theoretical derivation of Eqs. (8) and (9) is rather straightforward (*3–5*) and is not repeated here. It stems from simple electrostatic considerations and from the spatial uniformity of the Fermi level in the conductive catalyst film both at the catalyst–electrolyte and the catalyst–gas (i.e., catalytically active) interfaces (*3–5*). It is worth emphasizing that since the catalyst surface consists of a variety of crystallographic planes, one expects in general nontrivial spatial variations in WF and Volta potential Ψ. Equations (8) and (9) refer to the appropriately defined (10) average catalyst surface WF value. The local spatial variations in WF and Ψ are not expected to be very significant, however, in polycrystalline films with large (~1 μm) crystallites, such as the ones used in this and in other NEMCA studies, since the surface must consist primarily of low Miller index planes and in particular of the (111) plane.

As shown in Figs. 4a and 4b Eqs. (8) and (9) are valid for β''-Al_2O_3 solid electrolytes cells as well. Figure 4a depicts the transient catalyst potential V_{WR} and catalyst work function $e\Phi_W$ behavior during a galvanostatic transient, i.e., upon imposition of a fixed current between the catalyst and reference electrodes. As discussed below the induced WF change $\Delta e\Phi_W$ is due to Na spillover onto the catalyst surface. It can be seen that Eq. (9) is valid at steady-state and, to a good approximation, also during the transient. Figure 4b shows steady-state results obtained both under open-circuit and closed-circuit conditions. In the former case V_{WR} was varied by changing the C_2H_4/O_2 composition in the reactor and in the latter by varying the polarizing current with the catalyst exposed to O_2 and C_2H_4/O_2 mixtures.

In view of Figs. 4a and 4b in conjunction with similar results obtained with zirconia electrolytes (8) and also in view of the existing simple theoretical analysis (*3–5*) one can safely conclude that Eqs. (8) and (9) are

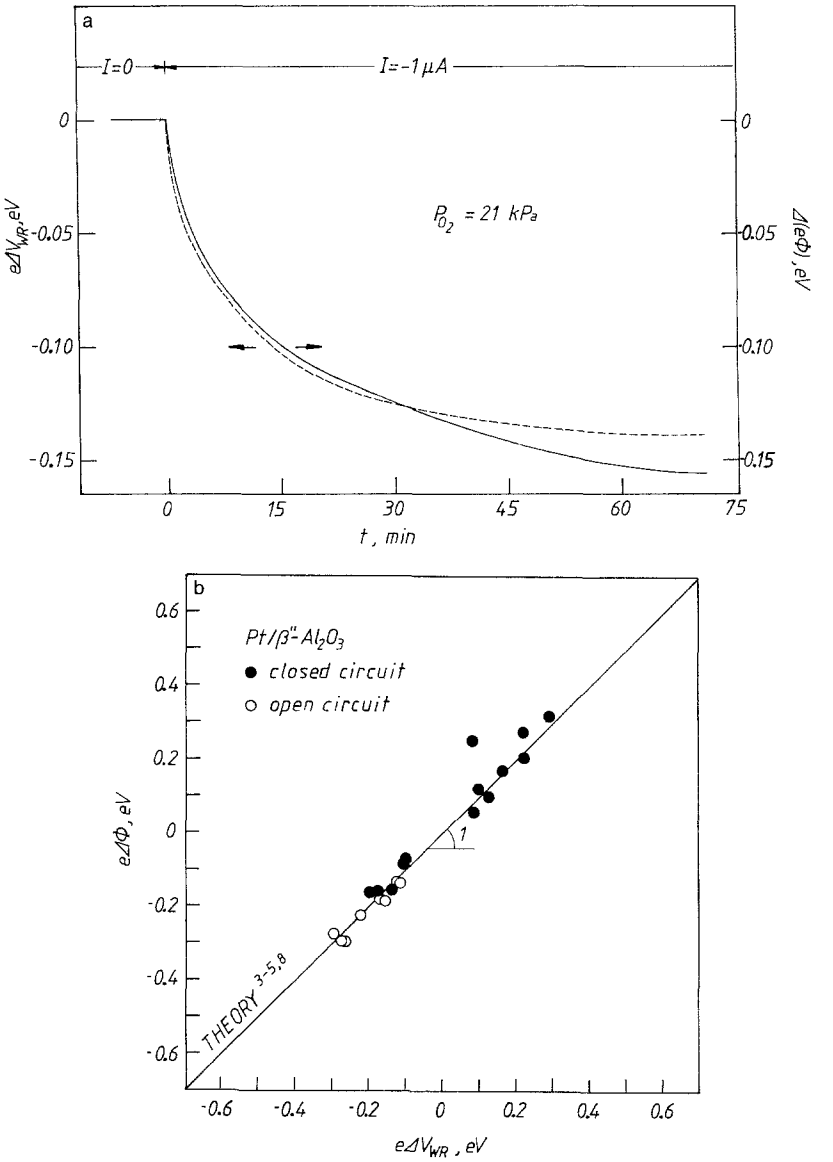

FIG. 4. Effect of ohmic-drop-free catalyst potential on the work function of the catalyst surface during a galvanostatic transient (a) and at steady state (b); T = 240°C.

always valid and that *solid electrolyte cells with metal electrodes are essentially work function probes of the gas-exposed electrode surfaces.*

Effect of Gas Composition on Catalyst Work Function

Figure 5 shows the effect of gaseous composition and temperature on the work function change of the Pt catalyst film in relation to its value when it was first exposed to P_{O_2} = 21 kPa. Open symbols on Fig. 5 correspond to data taken on the fresh catalyst (denoted hereafter C1) before exposure to electrochemical Na^+ pumping. These data, which show a quasilinear increase in WF with increasing $P_{O_2}/P_{C_2H_4}$, are in good qualitative agreement with the emf (V^o_{WR}) measurements of Ref. (*14*) (denoted by a dotted

line) which were obtained with a zirconia solid electrolyte and showed that $V_{WR}^{o} \sim \ln(P_{O_2}/P_{C_2H_4})$.

Filled symbols on Fig. 5 were obtained with the same catalyst after repeated exposure to electrochemical Na^+ pumping (hereafter denoted C2). It can be seen that increasing Na coverage on the catalyst surface (corresponding to $\Delta\theta_{Na} \approx 6.3 \times 10^{-3}$ as discussed below) induces important changes in the WF behavior. This is to be expected since the presence of alkalis on transition metal surfaces is known not only to cause notable (up to 3eV) WF decreases in vacuum, but also to magnify WF changes caused by adsorption of other adsorbates (*17*). This is exactly what Fig. 5 shows upon comparing catalysts C1 and C2. Thus the WF changes of C2 with changing $P_{O_2}/P_{C_2H_4}$ are much more pronounced. A quasilinear increase at relative low $P_{O_2}/P_{C_2H_4}$ is followed by a gradual asymptotic increase at high $P_{O_2}/P_{C_2H_4}$ values. The WF changes are more pronounced at higher temperatures. This is mainly because at lower temperatures strong ethylene adsorption takes place which inhibits oxygen adsorption and causes $e\Phi$ to remain low even for very high $P_{O_2}/P_{C_2H_4}$ ratios.

At 291°C and $P_{O_2}/P_{C_2H_4} = 240$, where most of the NEMCA experiments described below were carried out, the WF of catalyst C2

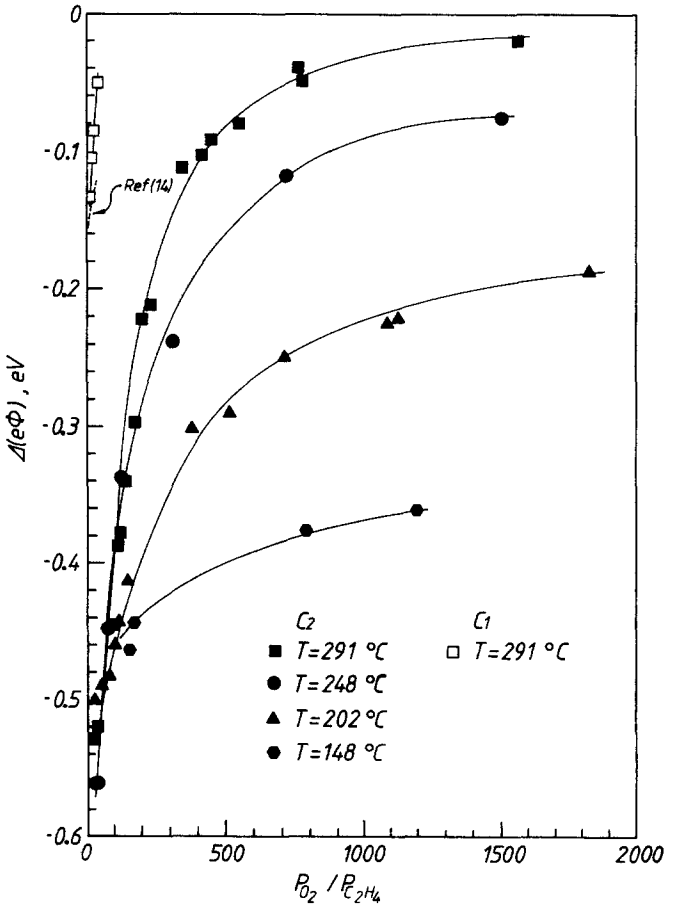

FIG. 5. Effect of gas composition on catalyst work function. Catalyst C1: P_{O_2} = 5 kPa. Catalyst C2: P_{O_2} = 15.3 kPa.

is by 0.19 eV lower than that of C1, causing significant differences in the kinetic behavior of C1 and C2 as discussed below. Using the literature value $P_0 = 5.3 \pm 0.2$ Debye ($= 1.75 \pm 0.07 \times 10^{-29}$ Cb · m) for the initial dipole moment of Na on Pt(111) (*16, 24*) and the Helmholz equation

$$P_0 = -\varepsilon_0(d\Phi/dN_{Na})_{N_{Na}\to 0}, \quad (10)$$

where $\varepsilon_0 = 8.85 \times 10^{-12}$ Cb^2/J · m, one computes that the Na surface density N_{Na} (adsorbed Na atoms/m^2) required to cause a 0.19 eV WF decrease is 9.6×10^{16}m^{-2}. Since there are 1.53×10^{19} Pt atoms/m^2 on the (111) plane, this corresponds to $\Delta\theta_{Na} = 6.3 \times 10^{-3}$; i.e., catalyst C2 has a higher Na coverage than C1. As discussed below the Na coverages for C1 and C2 are estimated, using Faraday's Law, to be 7.5×10^{-3} and 1.38×10^{-2}, respectively. Apparently this small Na coverage on C1 resulted from some nonelectrochemical Na spillover during catalyst preparation at high temperature. As shown below this Na contamination can be removed electrochemically.

It should be emphasized that calculating coverages from WF changes plus reported dipole moments is, in general, very risky. In the present case, however, one can be confident about the computed θ_{Na} values for two reasons: First because the θ_{Na} values involved are very small and well in the linear WF vs θ_{Na} region. Second because, as discussed below, one can start from an electrochemically cleaned surface and reproduce the catalytic activity, WF and θ_{Na} values of the catalyst film at the states C1 and C2 by electrochemically supplying Na at a rate (I/F) and by computing θ_{Na} from Faraday's Law and from the known value of the catalyst surface area.

It is worth mentioning that the above literature value of P_0 ($= 5.3$ Debye) for adsorbed Na/Pt(111) measured by Schröder and Hölzl under UHV conditions (*16, 24*), is in good qualitative agreement with the P_0 values obtained in the present work using galvanostatic transients, as discussed below.

Finally, it is noteworthy that, although *absolute* WF measurements by means of Kelvin probes are not reliable, mainly due to stray capacitance effects (*16, 25*), comparisons between various samples placed in the same geometric configuration are possible. After experimenting with a large number of Pt/$ZrO_2(Y_2O_3)$, Pt foil and Pt/β''-Al_2O_3 samples exposed to $P_{O_2} = 21$ kPa at $T = 240$°C, we have reached the conclusion that there exist significant (0.2–0.9 eV) systematic differences between the three work function values. This point needs further investigation using UPS or thermionic emission WF measurements.

Exchange Current Density

Figure 6 shows typical Tafel plots both for anodic ($I > 0$) and cathodic ($I < 0$) operation. The theory of using overpotential (η) vs current (I) data to extract the exchange current I_0, which plays a key role in determining the magnitude of the NEMCA enhancement factor Λ, has been described elsewhere (*3, 4*). As shown in Fig. 6 it is $I_0 = 1.4$ μA at 291°C, where most of the NEMCA experiments were carried out. Thus the exchange current density $i_0 = I_0/A$, where A is the superficial catalyst–solid electrolyte interface, is 0.7 μA/cm^2.

The anodic and cathodic transfer coefficients α_a and α_c, extracted from the slopes of the Tafel plots, are both rather low, i.e., 0.09 each. It is difficult to interprete these low transfer coefficient values on the basis of the classical theory of electrocatalytic reactions (*26*) if the kinetics of the dominant electrocatalytic reaction, i.e.,

$$Na^+(\beta''\text{-}Al_2O_3) + e^- \leftrightharpoons Na(Pt), \quad (11)$$

are rate limiting. It is likely that surface diffusion of Na on Pt, influenced by the strong electrostatic repulsion of the Na-compensating charge dipoles, plays an important role and leads to the observed low transfer coefficient values. This point needs further experimental and theoretical investigation but does not affect in any direct way the present work since it is only the order of

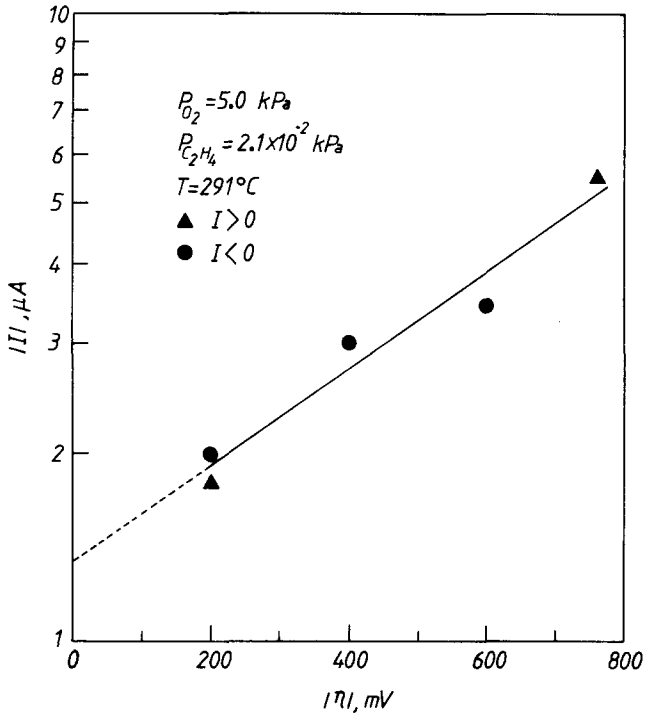

FIG. 6. Tafel plots for the catalyst–solid electrolyte interface.

magnitude of the exchange current I_0 which is relevant for the estimation of the enhancement factor Λ (*3*, *4*).

Catalyst Surface Area

Figure 7 shows typical isothermal surface titration results, i.e., it depicts the amount of chemisorbed oxygen remaining on the catalyst surface as a function of time of exposure to He, (t_{He}), after initial exposures to P_{O_2} = 21 kPa for t_{O_2} = 5 and 10 min. The observed logarithmic dependence, indicative of a pseudo-first-order desorption process, is in agreement with previous studies with Pt/ZrO_2 (*21*). The extrapolated N_O value, corresponding to t_{He} = 0, is 1.1 × 10^{-6} g-atom O. The oxygen desorption apparent rate constant K_d, computed from the slopes of Fig. 7, is 2.15 ± 0.15 × 10^{-2} s^{-1} at 590°C, in reasonable agreement with previous studies (*21*). As shown on Fig. 7, increasing the O_2 exposure time t_{O_2} has a small

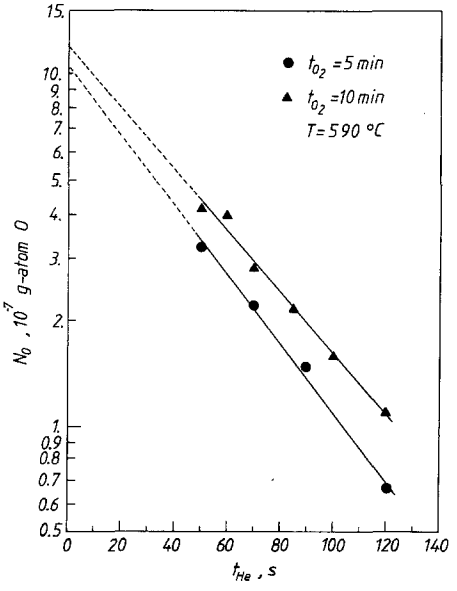

FIG. 7. Typical results of surface titrations during oxygen desorption after two different catalyst exposures to O_2.

increasing effect on the amount of chemisorbed oxygen (*21*), although the experiments were conducted under temperature conditions where no distinct second CO_2 peak, corresponding to PtO_2 (*21, 27, 28*) appears.

On the basis of the reactive oxygen uptake $N_O = 1.1 \times 10^{-6}$ g-atom O and assuming a one-to-one O to surface Pt ratio and a Pt surface density $N_{Pt} = 1.53 \times 10^{19}$ atoms/m^2 one estimates the catalyst surface area A to be 4.25×10^{-2} m^2.

Regular (Open-Circuit) Kinetic Behavior

In order to understand better the NEMCA effect on the kinetics of C_2H_4 oxidation it is important to study first the open-circuit ($I = 0$) kinetic behavior. There have been several kinetic studies of C_2H_4 oxidation on Pt (*3, 14, 29–33*). Two of them were performed on similar Pt films deposited on stabilized ZrO_2 (*3, 14*). It was found that for temperatures above 250°C the reaction rate r_o (g-atoms O/s) can be approximated well by

$$r_o = KK_{ad}P_{C_2H_4}P_{O_2}/(KP_{C_2H_4} + K_{ad}P_{O_2}), \quad (12)$$

where the subscript "o" refers to regular (open-circuit) catalytic activity. This expression, together with the solid electrolyte potentiometric (SEP) emf measurements had been interpreted quantitatively by the kinetic scheme

$$1/2 \left\{ \begin{array}{ll} O_2(g) + S \xrightarrow{K_{ad}} S \cdot O_2 & (13) \\ S \cdot O_2 + S \longrightarrow 2S \cdot O & (14) \end{array} \right\}$$

$$C_2H_4(g) + S \cdot O \xrightarrow[Pt]{K} P \xrightarrow{5/2\ O_2} 2CO_2 + 2H_2O, \quad (15)$$

where S denotes a Pt surface site, step (14) is assumed very fast, and P is a reactive intermediate which is rapidly oxidized by gaseous or adsorbed oxygen. The nature of such an intermediate has been investigated in a number of recent spectroscopic studies (*34–36*). It is likely that the first step in (*15*) is not purely of the Eley–Rideal type and that C_2H_4 adsorbs at a low coverage which is linear in $P_{C_2H_4}$. This is supported both by the surface titration experiments and also by the kinetic behavior at $T < 250$°C, as shown on Fig. 8, which is similar to that observed in that temperature range by Carberry (*30, 31*), Cant and Hall (*29*), and Hawkins and Wanke (*32*) on supported Pt catalysts. The rate maxima with increasing $P_{C_2H_4}$ are strongly indicative of competitive chemisorption of C_2H_4 and oxygen. It was found that by extending the kinetic scheme of Eqs. (13), (14), and (15) to include competitive equilibrium ethylene chemisorption one can describe adequately the kinetic behavior in that temperature range (*37*). The dashed lines on Fig. 8 result from this extended kinetic model. The extracted values for the C_2H_4 adsorption equilibrium constant $K_{C_2H_4}$ conform to

$$\ln(K_{C_2H_4}/\text{kPa}^{-1}) = -18.5 + 9400/T. \quad (16)$$

This expression shows that, indeed, at 291°C, where the simplified rate expression (12) is used, the C_2H_4 coverage is less than 0.08 for $P_{C_2H_4} < 0.5$ kPa, even in the absence of adsorbed O. The algebraic part of this kinetic model extension is omitted here since it is rather straightforward and since the NEMCA experiments were conducted at 291°C where the kinetic scheme of Eqs. (13), (14), and (15) and corresponding rate expression (12) are quite adequate, at least over the gaseous composition range investigated, i.e., 5 Pa $< P_{C_2H_4} <$ 600 Pa and 0.6 kPa $< P_{O_2} <$ 15 kPa. This is shown by the solid curve on Fig. 8 and also on Fig. 9 where the data are plotted against the linearized form of Eq. (12) for both catalysts C1 and C2, i.e., both before and after electrochemical Na contamination of the surface.

On the fuel-lean side ($KP_{C_2H_4} \ll K_{ad}P_{O_2}$) oxygen adsorption is near equilibrium and step (15) is rate limiting. In this case Eq. (12) reduces to

$$r_o = KP_{C_2H_4}. \quad (17)$$

The NEMCA study of C_2H_4 oxidation on Pt using zirconia as the solid electrolyte (*3,*

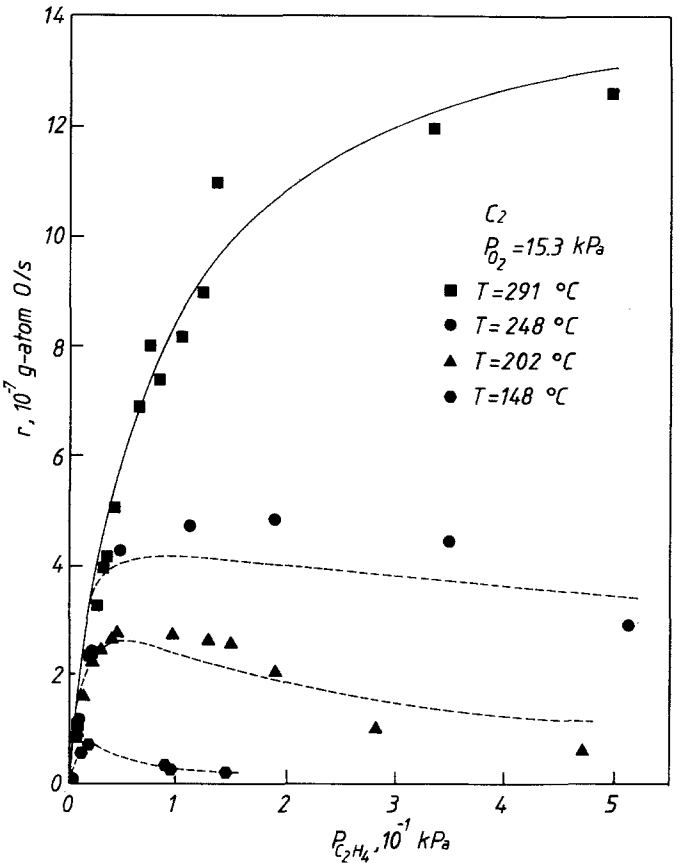

FIG. 8. Effect of $P_{C_2H_4}$ and temperature on the open-circuit catalytic rate; solid curve from Eq. (12), dashed curves from the extended kinetic model; see text for discussion.

5) has shown that it is in the fuel-lean side that the NEMCA-induced catalytic rate enhancement is dramatic, since K is strongly dependent on varying catalyst WF, whereas K_{ad} is rather insensitive. On the fuel-rich side ($KP_{C_2H_4} \gg K_{ad}P_{O_2}$) the surface oxygen coverage is low, the rate is controlled by oxygen adsorption, and Eq. (12) reduces to

$$r_o = K_{ad}P_{O_2}. \quad (18)$$

It is worth mentioning that within the framework of the kinetic model proposed in Refs. (*3, 14, 15*) the oxygen coverage θ_O can be computed from

$$\theta_O = (K_{ad}P_{O_2}/KP_{C_2H_4}) / [1 + (K_{ad}P_{O_2}/KP_{C_2H_4})]. \quad (19)$$

Table 1 presents the least-squares value of K and K_{ad} for catalysts C1 and C2 and compares them with previous values obtained on $Pt/ZrO_2(Y_2O_3)$ electrolytes (*3, 14, 15*). There is a striking increase in K and a concomitant striking decrease in K_{ad}, which makes the measured turnover rates to be comparable for both systems. Yet this pronounced difference makes it experimentally much more difficult to work on the fuel-lean side ($KP_{C_2H_4} \ll K_{ad}P_{O_2}$), where the NEMCA effect is dramatic, with Pt/β''-Al_2O_3 than with $Pt/ZrO_2(Y_2O_3)$. The origin of this significant difference is not obvious but could be related to the large systematic difference observed in the WF of Pt/β''-Al_2O_3 vs $Pt/ZrO_2(Y_2O_3)$. The decrease in K_{ad} is difficult to interpret in view of the fact that the

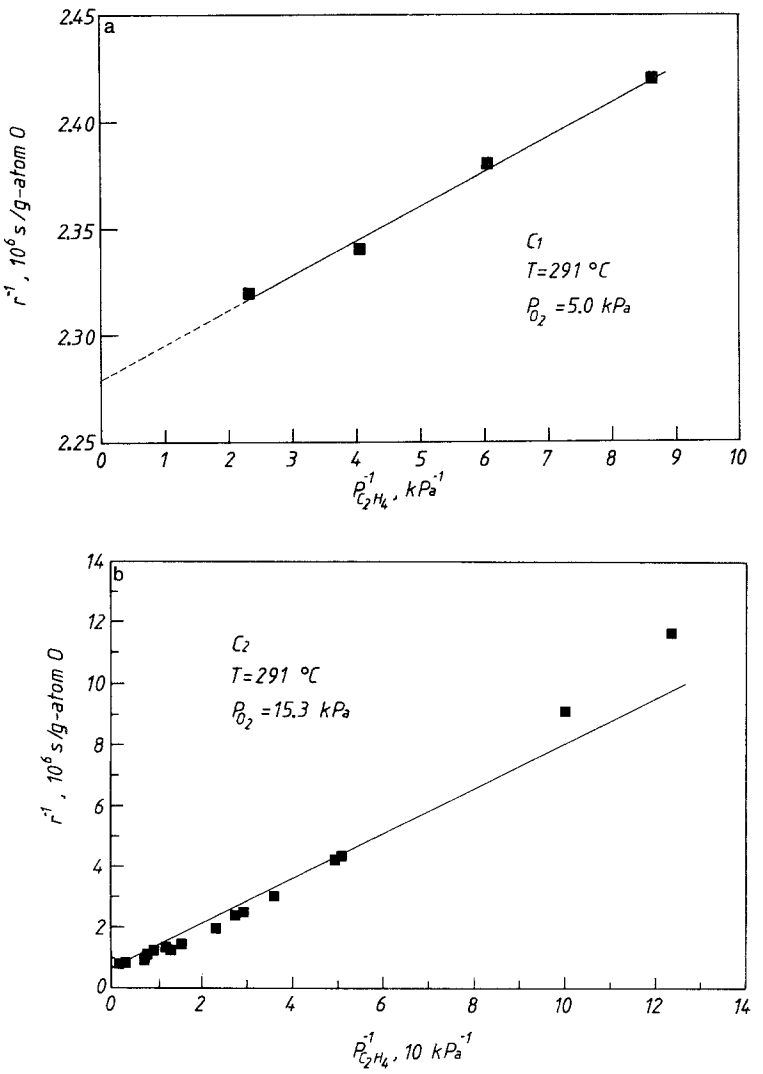

FIG. 9. Fitting of the linearized form of Eq. (12) to the open-circuit kinetic data at T = 291°C for catalysts C1 (a) and C2 (b).

presence of alkalis is known to enhance, in general, the sticking coefficient of oxygen on transition metal surfaces (*17*).

Comparison between catalysts C1 and C2 is much more straightforward. The lower, by approximately 0.19 eV, WF of C2 in comparison to C1 (Fig. 5) causes a fourfold decrease in K and has practically no effect on K_{ad}. The effect is qualitatively the same with that observed with $Pt/ZrO_2(Y_2O_3)$ (Refs. (*3*, *5*, *8*)).

NEMCA Behavior: Transients

Figure 10 shows a typical galvanostatic and potentiostatic transient. At the start of the experiment the circuit is open and the steady-state (regular) catalytic rate is 5.7×10^{-7} g-atom O/s with a corresponding V°_{WR} value of -430 mV. At time $t = 0$ the galvanostat is used to apply a constant current $I = -20$ μA between the catalyst and the counter electrode. Sodium ions Na^+ are

TABLE 1

Catalyst Surface Areas and Kinetic Constants

Catalyst film:	$Pt/(ZrO_2)$ Ref. (3)	$Pt/(ZrO_2)$ Ref. (3)	$Pt/(ZrO_2)$ Ref. (3)	$Pt/(ZrO_2)$ Ref. (14)	$Pt/(\beta''\text{-}Al_2O_3)$ C1	$Pt/(\beta''\text{-}Al_2O_3)$ C2
Reactive oxygen uptake N_O/g-atom O:	8.8×10^{-8}	4.2×10^{-9}	4.8×10^{-8}	1.6×10^{-6}	1.1×10^{-6}	1.1×10^{-6}
K/s^{-1} (T = 291°C):	120	67	100	250	5560	1230
K_{ad}/s^{-1} (T = 291°C):	240	1190	1300	180	8	9.2
Turnover frequency/s^{-1} at T = 291°C, P_{O_2} = 15.3 kPa, $P_{C_2H_4}$ = 0.5 kPa:	0.6	0.3	0.5	1.2	1.2	1.1

pumped onto the catalyst surface at a rate $(I/F) = 2.1 \times 10^{-10}$ g-atom/s. This causes a 66% decrease in catalytic rate which drops to 2.1×10^{-7} g-atom O/s. The steady-state change in catalytic rate $\Delta r = -3.6 \times 10^{-7}$ g-atom/s is 1720 times higher than the rate of supply of Na^+. The corresponding enhancement factor Λ defined, as in previous NEMCA studies (*1–10*), from $\Lambda = \Delta r/(I/2F)$ is 3430. At the same time the catalyst potential (and work function) decreases in a complex manner. The catalytic rate transient is essentially complete before the appearance of the second break in the catalyst potential transient at $V_{WR} = -900$ mV. This is in good agreement with the observed steady-state behavior described below.

The rate relaxation time constant τ, defined as in previous NEMCA studies (*1–10*), as the time required for the catalytic rate change to reach 63% of its final value, is 250 s. This is in reasonably good agreement with

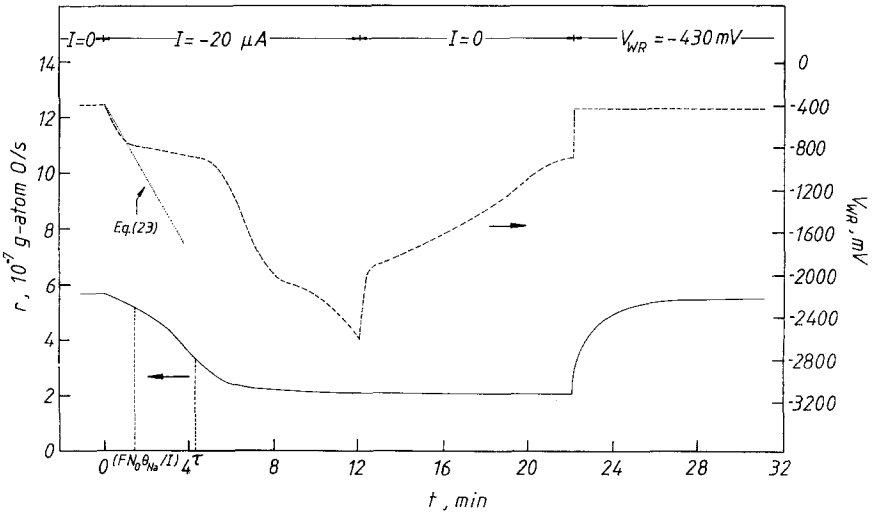

FIG. 10. Rate and catalyst potential response to application of negative current (Na supply to catalyst); Potentiostatic restoration of initial state; T = 291°C, P_{O_2} = 5.0 kPa, $P_{C_2H_4} = 2.10 \times 10^{-2}$ kPa; see text for discussion.

the time ($FN_O\theta_{Na}/I$ = 80 s) required for a Na coverage change of 0.0156, computed from the corresponding $\Delta(e\Phi)$ value (−0.47 eV), the independently measured catalyst surface area (4.25×10^{-2} m^2) and the literature initial dipole moment of Na/Pt(111), i.e., $P_0 = 1.75 \times 10^{-29}$ Cb · m (*16, 24*) through the Helmholz equation. Before analyzing this formally a simple but important point needs clarification:

The dominant cathodic electrocatalytic reaction (11) produces Na adsorbed on the Pt surface, which has been denoted by Na(Pt). As shown below, initial dipole moments obtained in the present work are in very good agreement with corresponding literature values for Na/Pt(111) obtained under UHV conditions. This implies that Na(Pt) formed in the present work by electrochemically supplying Na^+ through the β''-Al_2O_3 solid electrolyte is not different from adsorbed Na formed by utilizing the classical alkali metal dispenser filament sources used in UHV studies (*17*). Now each Na adatom is known to carry a positive charge δ which for the Na/Pt(111) system has been estimated by EELS to be of the order of $(0.6)e$ (*16, 24*). Thus, since I is measured as an electronic current, one might question whether the rate of Na(Pt) formation is indeed I/F. However, this is indeed the case, since each Na(Pt), i.e., each $Na^{\delta+}$ which spills over the Pt surface is compensated by an equal and opposite screening electron charge—δ in the metal. This is because it follows from simple electrostatic considerations that no net average charge can be sustained on the catalyst–gas interface and any catalyst charge must be located at the catalyst–solid electrolyte interface (*3, 4*). It is exactly the $Na^{\delta+}$-compensating charge dipoles which alter the catalyst surface WF. Therefore the average electron charge required for each Na^+ extracted from the β''-Al_2O_3 and supplied as $Na^{\delta+}$ onto the catalyst surface, is $(1 - \delta) + \delta = 1$. Consequently the rate of Na supply to the catalyst surface is indeed I/F.

One can thus quantify the expected catalyst WF change during a galvanostatic transient as follows. First one uses Faraday's law and the known catalyst surface area to determine the evolution in time of the Na coverage θ_{Na},

$$\frac{d\theta_{Na}}{dt} = -\frac{N_{AV}(I/F)}{A \cdot N_{Pt}}, \tag{20}$$

where N_{AV} is Avogadro's number, A is the catalyst surface area (m^2), and $N_{Pt} = 1.53 \cdot 10^{19}$ atoms/m^2 is the surface Pt concentration of the Pt(111) plane. One can then combine Eq. (20) with the definition of $\theta_{Na}(=N_{Na}/N_{Pt})$ and with the differentiated Helmholz equation:

$$\frac{d(e\Phi)}{dt} = -\frac{eP_0}{\varepsilon_0} \cdot \frac{dN_{Na}}{dt} \tag{21}$$

to obtain

$$\frac{d(e\Phi)}{dt} = \frac{P_0 I}{\varepsilon_0 \cdot A}. \tag{22}$$

Substituting $P_0 = 1.75 \times 10^{-29}$ Cb · m, $I = -20$ μA and $A = 4.25 \times 10^{-2}$ m^2 one obtains

$$d(e\Phi)/dt = -5.80 \times 10^{-3} \text{ eV/s}, \tag{23}$$

which corresponds to the dotted straight line on Fig. 10 and is in excellent agreement with the initial slope of the catalyst work function (and potential) transient.

In view of this excellent agreement one may use galvanostatic transient diagrams such as Fig. 10 in conjunction with Eq. (22) to estimate dipole moments of dipoles formed by adsorbed species on metal surfaces. Thus from the initial slope $d(e\Phi)/dt$ in Fig. 10 and using Eq. (22) one obtains $P_0 = 6.4$ Debye ($=2.1 \times 10^{-29}$ Cb · m) in excellent agreement with the literature value of 5.3 Debye for Na/Pt(111) (*16, 24*).

Figure 10 also shows that when the circuit is opened ($I = 0$) the catalyst potential starts increasing but the reaction rate does not change appreciably. This is different from the behavior observed with O^{2-} conducting solid electrolytes (1–10) and must be due to the fact that the spillover oxygen anions can react with the fuel (e.g., C_2H_4, CO) albeit at

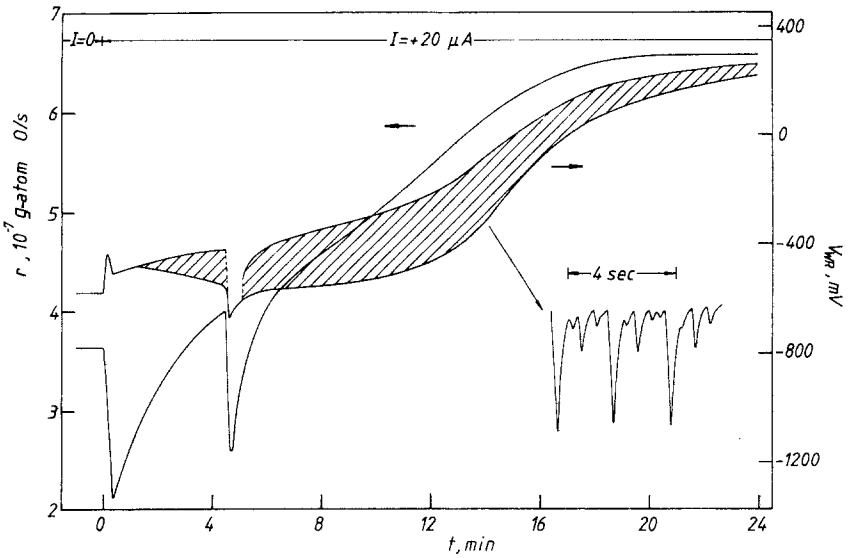

FIG. 11. Rate and catalyst potential response to application of positive currents (Na removal from catalyst) and induced oscillatory behavior; T = 291°C, P_{O_2} = 5.0 kPa, $P_{C_2H_4}$ = 8.2 × 10^{-2} kPa.

a slow rate (*3*), whereas Na(Pt) cannot be scavenged from the catalyst surface.

However, as shown in Fig. 10, when the potentiostat is used to impose the initial catalyst potential (−430 mV) and work function, then the catalytic rate is restored within 100–150 s to its initial value, since Na(Pt) can now be pumped again as Na^+ into the β''-Al_2O_3 structure. Thus the phenomenon is reversible. It is clear then that potentiostatic operation is advantageous for this system, while both potentiostatic and galvanostatic operation offer different but comparable advantages with O^{2-} conducting solid electrolytes (*1–10*).

As shown on Fig. 11, which depicts another galvanostatic transient, one can use NEMCA to induce catalyst potential and rate oscillations, as in the case of CO oxidation on Pt (*2*).

NEMCA: Steady-State Behavior

Figure 12 shows the effect of catalyst potential V_{WR} and of change in catalyst work function $e\Phi_W$ on the rate of C_2H_4 oxidation. Regarding the WF scale, we have chosen to present only WF changes, relative to the catalyst WF at a maximum activity (θ_{Na} = 0), rather than absolute WF values since, as mentioned previously, Kelvin probes cannot provide reliable absolute WF values but only very reliable changes in work function.

As in previous NEMCA studies (*1–10*) there is a V_{WR} region where the catalytic rate depends exponentially on catalyst potential and work function, i.e.,

$$\ln(r/r_o) = \alpha e(V_{WR} - V^*_{WR})/k_bT \quad (24a)$$

or, equivalently (Eq. 9),

$$\ln(r/r_o) = \alpha e(\Phi_W - \Phi^*_W)/k_bT, \quad (24b)$$

where V^*_{WR} and Φ^*_W are catalyst- and reaction-specific constants. The parameter α has the value 0.13. Thus, similarly to the NEMCA behavior using O^{2-} conductors (*3*), C_2H_4 oxidation on Pt exhibits "electrophobic" behavior (*4, 8*), i.e., the catalytic rate increases with increasing catalyst work function.

The catalyst potential region where the above exponential rate change takes place is the same with the one in the galvanostatic transient on Fig. 10 and underlines again that the key parameter for describing the NEMCA effect is not the current but rather the catalyst potential and work function.

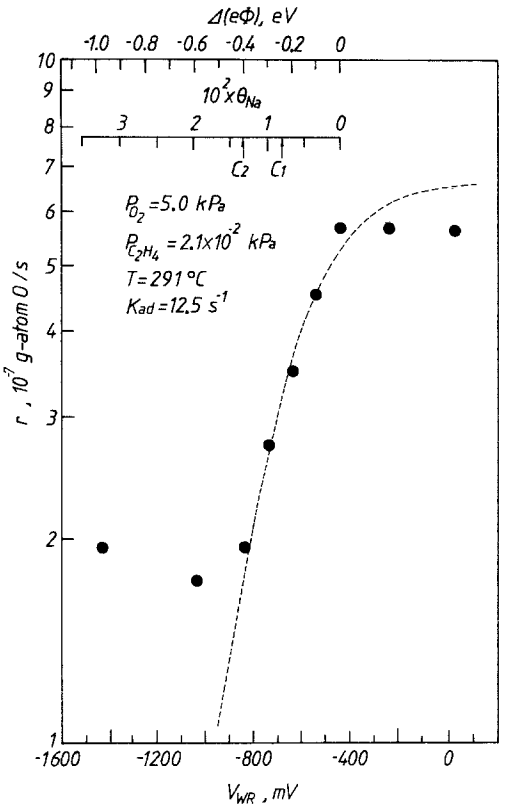

FIG. 12. Effect of catalyst potential V_{WR}, work function $e\Phi_W$ and corresponding Na coverage on the rate of C_2H_4 oxidation. Dotted line from Eqs. (12) and (27).

The inserted θ_{Na} abscissa in Fig. 12 is constructed on the basis of the following form of the Helmholz equation:

$$\Delta\Phi = -(N_{Pt}P_0/\varepsilon_0)\theta_{Na}, \qquad (25)$$

which, as shown in the previous section, is in very good agreement with experiment. It is worth noting that θ_{Na} changes of the order of 1% suffice to reversibly change the catalytic rate by a factor of 3.

The dashed line in Fig. 12 results from the kinetic scheme of reactions (13), (14), and (15) and the resulting kinetic expression (12) on the assumption that, as in the case of C_2H_4 oxidation on $Pt/ZrO_2(Y_2O_3)$ (*3*), it is only K which is affected by the changing WF while the oxygen adsorption rate constant K_{ad} remains unaffected. The validity of this assumption is strongly supported by Fig. 13. Indeed by solving the rate expression (12) in terms of K one obtains:

$$K = r/[P_{C_2H_4} - (rP_{C_2H_4}/K_{ad}P_{O_2})]. \qquad (26)$$

Using this equation and the raw data of Fig. 12 one obtains Fig. 13 which shows that, in the range -830 mV $< V_{WR} < -430$ mV, K increases exponentially with V_{WR}:

$$\ln(K/K_o) = \alpha' e(V_{WR} - V^*_{WR})/k_bT \qquad (27a)$$

or, equivalently,

$$\ln(K/K_o) = \alpha' e(\Phi_W - \Phi^*_W)/k_bT, \qquad (27b)$$

where $\alpha' = 0.28$. The dashed lines both in Figs. 12 and 13 were constructed using a K_{ad} value of 12.5 s^{-1}. This is somewhat higher than the K_{ad} values (8 and 9.2 s^{-1}) given in Table 1 for catalysts C1 and C2 respectively but provides a better fit to the NEMCA data. This is very likely due to the fact that in

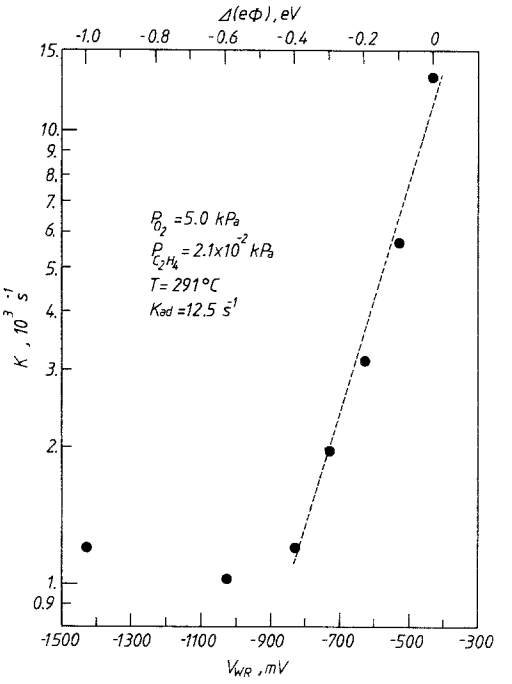

FIG. 13. Effect of catalyst potential V_{WR} and of corresponding work function value on the kinetic constant K of C_2H_4 oxidation on $Pt/(\beta''\text{-}Al_2O_3)$. Dotted line from Eq. (27); see text for discussion.

TABLE 2

Measured and Computed (Eq. (6)) Λ Values

$r(I = 0) = 5.66 \times 10^{-7}$ g-atom O/s				
$r/10^{-7}$ g-atom O/s	$I/\mu A$	$\Delta r/10^{-7}$ g-atom O/s	Λ_{exp}	Λ_{th} (Eq. (6))
3.49	−2	−2.17	20950	26600
1.93	−3	−3.73	24000	25500

using the open-circuit kinetic data to extract the kinetic constant values shown on Table 1, one should have taken into account a posteriori the effect of changing gaseous composition and concomitant change in WF (Fig. 5) on the extracted K value. It should be noted that the K value of the "contaminated" catalyst C2 corresponds to the plateau in Fig. 13.

In view of Eq. (27) one may conclude that the fact that the logarithm of the rate increases with an apparent slope smaller than that in the case where ZrO_2 is used as the ion donor is not only due to the fact that the ratio K/K_{ad} is much lower on $Pt/ZrO_2(Y_2O_3)$ than on Pt/β''-Al_2O_3, thus making it here much more difficult experimentally to work under fuel-lean conditions where the NEMCA effect is much more pronounced. The data show that the NEMCA coefficient α' for the kinetic constant K is lower for Pt/β''-Al_2O_3 ($=0.28$) than for $Pt/ZrO_2(Y_2O_3)$ (typically 0.5–1). A possible explanation for this difference is given in the next section where the origin of the "threshold" WF value below which K becomes insensitive to WF (Figs. 12 and 13) is also discussed.

DISCUSSION

The main finding of this work is that the NEMCA effect is not limited to the use of O^{2-} conductors (*1–7*) but can also be induced using Na^+ conductors, such as β''-Al_2O_3. In the following we discuss similarities, which are numerous, and differences.

A second finding is that the ohmic-drop-free potential of β''-Al_2O_3 solid electrolyte cells with one electrode also functioning as a catalyst can be used as an *in situ* work function probe of the catalyst surface. In different terms β''-Al_2O_3 cells can also be used for solid electrolyte potentiometric studies (*6, 38, 39*). In view of the present WF results (Fig. 4) and of the similar recent theoretical (*3–5*) and experimental (*8*) findings about the WF probing capacity of solid electrolyte cells it becomes obvious that SEP is, in essence, an *in situ* work function measurement for the gas-exposed catalyst surface. One can still use SEP to extract information about surface activities provided the nature of the electrocatalytic reaction is well known but, even when this is not the case, the cell emf still provides a direct measure of the difference in the work function between the two gas-exposed electrode surfaces. Several aspects of the SEP literature reviewed in Refs. (*6, 38, 39*) can be reexamined in light of these new findings and a paper on this subject is in preparation (*40*).

Electrocatalytic Reactions and Sodium Spillover

The dominant electrocatalytic reaction which induces the NEMCA effect in β''-Al_2O_3 cells is

$$Na^+(\beta''\text{-}Al_2O_3) + e^- \rightleftharpoons Na(Pt). \quad (11)$$

This electrocatalytic reaction takes place at the gas–metal–solid electrolyte three-phase boundaries. The thus-produced partially charged adsorbed Na atoms together with their compensating charge in the metal spill over the entire catalyst surface. The

driving force is the strong electrostatic dipole repulsion (*17*). This repulsion apparently forces the dipoles to spread uniformly over the catalyst surface and induce dramatic changes in catalytic activity even at very low coverages (Fig. 13).

In addition to the dominant electrocatalytic reaction (*11*) other parallel electrocatalytic reactions may also be taking place to a limited extent at the three-phase boundaries:

$$H^+ + e^- \leftrightharpoons H(ad) \quad (28a)$$

$$2O(ad) + 4e^- \leftrightharpoons 2O^{2-} \quad (28b)$$

$$H^+ + O(ad) + e^- \leftrightharpoons OH(ad) \quad (28c)$$

$$H^+ + OH(ad) + e^- \leftrightharpoons H_2O. \quad (28d)$$

These reactions must play a significant role only after depletion of Na^+ and Na(Pt) has taken place at the three-phase boundaries. This could happen, for example, at the counter electrode after extended negative current application. Although no serious cell irreversibility problems were encountered in this study over a period of several months (apparently due to the very small currents and reversed cell operation employed) it is clear that one could eliminate such problems in future studies by maintaining the counter electrode in contact with molten Na.

The Magnitude of Λ

As in previous studies of the NEMCA effect (*1–10*), the magnitude of the enhancement factor Λ can be estimated from:

$$\Lambda \approx 2Fr_o/I_0. \quad (6)$$

Equation (6) has been derived theoretically elsewhere (*3, 4*). It shows that in order to observe a pronounced non-Faradaic rate enhancement ($|\Lambda| \gg 1$), one needs a highly polarizable (low I_0) catalyst–solid electrolyte interface.

In the present study Λ values of the order of 10^3–5×10^4 were measured. The very good agreement between experiment and Eq. (6) is shown in Table 2 and also in Fig. 14

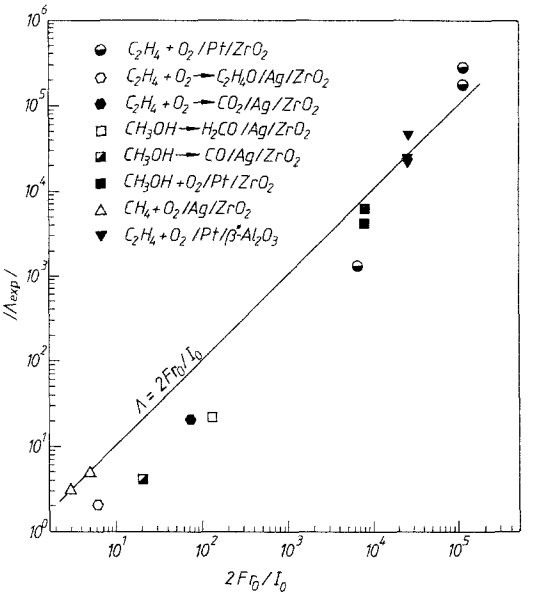

FIG. 14. Comparison of predicted and measured enhancement factor Λ values for the catalytic reactions found to exhibit the NEMCA effect (Refs. (*1–10*) and present work).

which also summarizes Λ results obtained in previous NEMCA studies (*1–10*). The r_o value used in Table 2, for the computation of Λ_{th}, equal to $1.93 \cdot 10^{-7}$ g-atom O/s, corresponds to the lower plateau value on Fig. 12 (catalyst C2) since it follows from the derivation of Eq. (6) that "r_o" must be selected as the minimum rate value (*3, 4*). A slight algebraic modification of Eq. (6), i.e., $\Lambda = (2Fr_o/I_0)(1 - |I_o/I|)$, is needed if one chooses to use as "r_o" the $r(I = 0)$ value, even when this value is not the minimum one.

The Magnitude of τ

The observed catalytic rate relaxation time constants τ during galvanostatic transients can be approximated reasonably well (Fig. 10) by

$$\tau \approx (N_{Pt}/N_{AV})FA\theta_{Na}/I \quad (29a)$$

obtained from Eq. (20) or, equivalently, by

$$\tau \approx N_O F\theta_{Na}/I \quad (29b)$$

or, in terms of the induced WF change (Eq. 22), by

$$\tau \approx \frac{\varepsilon_0 A \Delta(e\Phi)}{P_0 I}. \qquad (29c)$$

Equation (29) shows clearly that the entire catalyst surface changes its catalytic properties. Equation (29b) is very similar to $\tau \approx 2FN_O/I$ which provides a good estimate for the case of O^{2-} conducting solid electrolytes (*1–7*).

The Origin of NEMCA

The above observations show clearly that the NEMCA effect induced by β''-Al_2O_3 is due to Na spillover onto the Pt catalyst surface. Thus, essentially, the solid electrolyte allows for a controllable, measurable, and reversible dosing of Na onto the catalyst surface. This is similar with the case of $ZrO_2(Y_2O_3)$ which acts as a donor of oxygen anions onto the catalyst surface (*1–10*).

The fact that very small Na coverages (e.g., $\theta_{Na} = 0.015$) suffice to induce a pronounced (up to 70%) decrease in the rate of C_2H_4 oxidation (i.e., the Na^+ "toxicity" is (0.70)/(0.015) = 47) rules out the possibility of any geometric interpretation of NEMCA.

The observed exponential dependence of catalytic rate (Fig. 12) and of the kinetic constant K (Fig. 13) on catalyst work function provides evidence that, as in the case of O^{2-} conductors (*1–10*), NEMCA can be interpreted as a "long range" electronic effect. For if the effect were localized only to those Pt atoms immediately adjacent to adsorbed Na then, for $\theta_{Na} = 0.015$, one would expect at most a rate decrease of 10%, i.e., a factor of seven smaller than the observed one. The observed behavior is strongly reminiscent of the IRS work of Uram *et al.* (20) who studied the CO + K/Ni(111) system and concluded that a single K atom can influence as many as 27 coadsorbed CO molecules. Long-range electronic effects have been also predicted theoretically for some adsorbates on metal surfaces (*41*) and have been invoked to explain the dependence of the sticking coefficient of O_2 on alkali-doped Ge, which was found to depend exponentially on the alkali-induced $e\Phi$ change, regardless of alkali type (*42*). However, alternative "short-range" explanations of NEMCA cannot be ruled out before using TPD and scanning tunneling microscopy (*43*) as an atomic scale $e\Phi$ probe. For example it is possible that, if the spillover ions were producing a short-range effect but their mobility were so high that their average surface migration time from one catalytic site to another were shorter than the reaction time of the catalytic reaction, then one would macroscopically observe a "long-range" effect (*44*). It is also very likely that there is no universal answer and that the long- or short-range electronic nature of NEMCA is catalyst- and spillover ion-specific.

The observed exponential increase in the Eley–Rideal kinetic constant K can be interpreted as follows within the framework of a long-range effect: Spillover $Na^{\delta+}$-compensating charge dipoles cause a more or less uniform decrease in catalyst surface work function and a concomitant increase in the binding strength of the Pt–oxygen bond, cleavage of which is rate limiting (*3*). Chemisorbed atomic oxygen is an electron acceptor (*45*) and, therefore, a WF decrease will strengthen the Pt–oxygen bond. In fact, according to early theoretical considerations of Boudart (*12*), it should be

$$\Delta(-\Delta H_{ad,O}) = -(n/2)\Delta e\Phi, \qquad (30)$$

where $-\Delta H_{ad,O}$ is the oxygen heat of adsorption and $n = 2$ is the number of binding electrons. If the nature of the activated complex is not changing substantially with varying WF, then a linear increase in $-\Delta H_{ad,O}$ will cause a linear increase in activation energy, a concomitant less pronounced increase in preexponential factor due to the decreased entropy of the more tightly bound oxygen (*3*), and an overall exponential decrease in catalytic rate, as experimentally observed, i.e.,

$$\ln(K/K_o) = \alpha' e(\Phi - \Phi^*)/k_b T. \qquad (27)$$

The origin of the observed deviation of the experimental data from Eq. (27) at very low WF values (Fig. 13) is not obvious. A similar "threshold" WF value below which the catalytic rate becomes insensitive to WF changes was observed for the same reaction with O^{2-} solid electrolytes as spillover ion donors (*3*). Lateral interactions have been invoked to explain similar abrupt heat of adsorption variations with $e\Phi$ in UHV studies (*46*). In the present system the observed behavior could be related to the formation of Na_2O, NaOH or Na_2CO_3 on the surface at very low WF values (*17*). Surface reactions leading to these compounds are very likely to occur in the presence of O_2, H_2O, and CO_2 in the reactor. Such reactions can explain why a constant, albeit very small (<1 μA), current is sustained at steady state even with potentiostatic operation. This current is probably a steady-state measure of the sum of the rates of Na_2O, NaOH, and Na_2CO_3 formation.

The fact that ln r levels off at high WF values (Fig. 12) is due to the transition from fuel-lean ($KP_{C_2H_4} < K_{ad}P_{O_2}$) to fuel-rich ($KP_{C_2H_4} > K_{ad}P_{O_2}$) conditions and to the concomitant rate transition from first order in C_2H_4 and zeroth order in O_2 to zeroth order in C_2H_4 and first order in O_2, as in the case of ZrO_2 anion donor (*3*).

The measured NEMCA coefficient α' is 0.28, i.e., lower than the corresponding values measured with the $Pt/ZrO_2(Y_2O_3)$ system, i.e., 0.5 to 1 (*3*). In view of the fact that Pt/β''-Al_2O_3 appears to have a WF significantly different than that of $Pt/ZrO_2(Y_2O_3)$ one can speculate that this difference is due to the lower value of the local density of states (LDOS) at the Fermi level for Pt/β''-Al_2O_3 vs $Pt/ZrO_2(Y_2O_3)$. Detailed numerical information about the distribution of the LDOS near the Fermi level for most metals can be found in Refs. (*47, 48*).

Indeed previous NEMCA studies (*1–10*) have provided some remote evidence for a correlation between α' and the LDOS at the Fermi level. The absolute value of the former is typically 0.3–1.0 for Pt-catalyzed reactions and 0.1–0.2 for Ag-catalyzed reactions. The corresponding LDOS values are 2.2 states/eV · atom for Pt and 0.27 states/eV · atom for Ag (*47, 48*). Unfortunately no reliable NEMCA coefficients are yet available for other transition metals such as Pd or Ni which have very high LDOS at the Fermi level (2.3 and 4.1 states/eV · atom, respectively). This hypothesis obviously requires further experimental investigation.

SUMMARY

The present results demonstrate that:

I. NEMCA is not limited to any specific type of solid electrolyte and is due to ion spillover.

II. Solid electrolyte cells are work function probes for the gas-exposed electrode surfaces.

It is quite interesting and encouraging that several key aspects of the NEMCA behavior using β''-Al_2O_3 as the ion donor under atmospheric pressure conditions (e.g., the adsorbed Na dipole moment) are consistent with the rich UHV literature on the interaction of alkalis with atomically clean transition metal surfaces (*17*). Although NEMCA has been studied so far for only approximately 12 reactions (*1–10*), it appears to be a general effect in heterogeneous catalysis with numerous potential theoretical and practical applications. Technological potential could emerge as more reactions are studied. Surface spectroscopic investigation of catalyst surfaces under NEMCA conditions is highly desirable, as it could elucidate many of the remaining open questions and provide new insights to the "electronic factor" component of heterogeneous catalysis.

ACKNOWLEDGMENTS

We thank Professor Budevski for the β''-Al_2O_3. Financial support by the VW Foundation of the Federal Republic of Germany and by the EEC Non-Nuclear Energy program is also gratefully acknowledged.

REFERENCES

1. Vayenas, C. G., Bebelis, S., and Neophytides, S., *J. Phys. Chem.* **92,** 5983 (1988).

2. Yentekakis, I. V., and Vayenas, C. G., *J. Catal.* **111,** 170 (1988).
3. Bebelis, S., and Vayenas, C. G., *J. Catal.* **118,** 125 (1989).
4. Neophytides, S., and Vayenas, C. G., *J. Catal.* **118,** 147 (1989).
5. Vayenas, C. G., Bebelis, S., Neophytides, S., and Yentekakis, I. V., *Appl. Phys. A* **49,** 95 (1989).
6. Lintz, H.-G., and Vayenas, C. G., *Angew. Chem.* **101,** 725 (1989): *Intl. Engl. Ed.* **28,** 708 (1989).
7. Vayenas, C. G., Bebelis, S., and Neophytides, S., *in* "Studies in Surface Science and Catalysis" (G. Centi and F. Trifiro, Eds.). Elsevier, Amsterdam/ New York, 1990.
8. Vayenas, C. G., Bebelis, S., and Ladas, S., *Nature (London)* **343,** 625 (1990).
9. Vayenas, C. G., Bebelis, S., Yentekakis, I. V., Tsiakaras, P., and Karasali, H., *Platinum Met. Rev.* **34,** 122 (1990).
10. Vayenas, C. G., and Neophytides, S., *J. Catal.*, in press (1990).
11. Pritchard, J., *Nature (London)* **343,** 592 (1990).
12. Boudart, M., *J. Amer. Chem. Soc.* **74,** 3556 (1952).
13. Farrington, G. C., Dunn B., and Thomas, J. O., *in* "High Conductivity Solid Ionic Conductors" (T. Takahashi, Ed.), pp. 327–365. World Scientific, Singapore, 1989.
14. Vayenas, C. G., Lee, B., and Michaels, J. N., *J. Catal.* **66,** 36 (1980).
15. Vayenas, C. G., Georgakis, C., Michaels, J. N., and Tormo, J., *J. Catal.* **67,** 348 (1981).
16. Hölzl, J., and Schulte, F. K., *in* "Solid Surface Physics" (J. Hölzl *et al.*, Eds.), pp. 1–150. Springer-Verlag, Berlin, 1979.
17. Bonzel, H. P., *Surf. Sci. Reports* **8,** 43 (1987).
18. Heskett, D., *Surf. Sci.* **199,** 67 (1988).
19. Aruga, T., and Murata, Y., *Progr. Surf. Sci.* **31,** 61 (1989).
20. Uram, K. J., Ng, L., and Yates, J. T., Jr., *Surf. Sci.* **177,** 253 (1986).
21. Yentekakis, I. V., Neophytides, S., and Vayenas, C. G., *J. Catal.* **111,** 152 (1988).
22. Stoukides, M., and Vayenas, C. G., *J. Catal.* **64,** 18 (1980).
23. Besocke, B., and Berger, S., *Rev. Sci. Instrum.* **47**(7), 840 (1976).
24. Schröder, W., and Hölzl, J., *Solid State Commun.* **24,** 777 (1977).
25. Ritty, B., Wachtel, F., Manquenouille, R., Ott, F., and Donnet, I. B., *J. Phys. E: Sci. Instrum.* **15,** 310 (1982).
26. Bockris, J. O'M., and Reddy, A. K. N., "Modern Electrochemistry." Plenum, New York, 1973.
27. Peuckert, M., *J. Phys. Chem.* **89,** 2481 (1985).
28. Vayenas, C. G., and Michaels, J. N., *Surf. Sci.* **120,** L405–L1408 (1982).
29. Cant, N. W., and Hall, W. K., *J. Catal.* **16,** 220 (1970).
30. Carberry, J. J., *Kinet. Katal.* **18**(3), 562 (1977).
31. Carberry, J. J., *Acc. Chem. Res.* **18,** 358 (1985).
32. Hawkins, J. R., and Wanke, S. E., *Canad. J. Chem. Eng.* **57,** 621 (1979).
33. Sant, R., Kaul, D. J., and Wolf, E. E., *AIChE J.* **35**(2), 267 (1989).
34. Palmer, R. L., *J. Vac. Sci. Technol.* **12,** 1403 (1975).
35. Steininger, H., Ibach, H., and Lehwald, S., *Surf. Sci.* **117,** 685 (1982).
36. Berlowitz, P., Megiris, C., Butt, J. B., and Kung, H. H., *Langmuir* **1,** 206 (1985).
37. Despotopoulou, M., Diplom. Eng. Thesis, University of Patras, 1989.
38. Vayenas, C. G., *Solid State Ionics* **28–30,** 1521 (1988).
39. Stoukides, M., *I&EC Res.* **27,** 1745 (1988).
40. Bebelis, S., and Vayenas, C. G., in preparation.
41. Feibelman, P. J., and Hamann, D. R., *Surf. Sci.* **149,** 48 (1985).
42. Surnev, L., *Surf. Sci.* **11,** 458 (1981).
43. Binnig, G., and Rohrer, H., *Surf. Sci.* **126,** 236 (1983).
44. Yentekakis, I. V., personal communication.
45. Shustorovich, E., *Surf. Sci. Reports* **6,** 1 (1986).
46. Madden, H., Küppers, J., and Ertl, G., *J. Chem. Phys.* **58,** 3401 (1973).
47. Moruzzi, V. L., Janak, J. F., and Williams, A. R., *in* "Calculated Electronic Properties of Metals." Pergamon, New York, 1978.
48. Papaconstantopoulos, D. A., "Handbook of the Band Structure of Elemental Solids." Plenum, New York, 1986.